


Article

Effect of Grinding on Chrysotile, Amosite and Crocidolite and Implications for Thermal Treatment

Andrea Bloise ^{1,*} , Manuela Catalano ¹ and Alessandro Francesco Gualtieri ²

¹ Department of Biology, Ecology and Earth Sciences, University of Calabria, Via Pietro Bucci, I-87036 Rende, Italy; manuela.catalano@fis.unical.it

² Department of Chemical and Geological Sciences, University of Modena and Reggio Emilia, I-41121 Modena, Italy; alessandro.gualtieri@unimore.it

* Correspondence: andrea.bloise@unical.it; Tel.: +39-09-8449-3588

Received: 20 February 2018; Accepted: 26 March 2018; Published: 28 March 2018



Abstract: Nowadays, due to the adverse health effects associated with exposure to asbestos, its inertization is one of the most important issues of waste risk management. Based on the research line of mechano-chemical and thermal treatment of asbestos containing materials, the aim of this study was to examine the effects of dry grinding on the structure, temperature stability and fibre size of chrysotile from Balangero (Italy), as well as standard UICC (Union for International Cancer Control) amosite and standard UICC (Union for International Cancer Control) crocidolite. Dry grinding was accomplished in an eccentric vibration mill by varying the grinding time (30 s, 5 and 10 min). Results show a decrease in crystallinity, the formation of lattice defects and size reduction with progressive formation of agglomerates in the samples after the mechanical treatment. Transmission electron microscopy (TEM) results show that the final product obtained after 10 min of grinding is composed of non-crystalline particles and a minor residue of crystalline fibres that are not regulated because they do not meet the size criteria for a regulated fibre. Grinding results in a decrease of temperature and enthalpy of dehydroxylation (ΔH_{dehy}) of chrysotile, amosite and crocidolite. This permits us to completely destroy these fibres in thermal inertization processes using a lower net thermal energy than that used for the raw samples.

Keywords: asbestos; chrysotile; amosite; crocidolite; grinding

1. Introduction

The commercial term asbestos regards chrysotile (serpentine asbestos) and five fibrous amphiboles (actinolite asbestos, amosite, anthophyllite asbestos, crocidolite and tremolite asbestos) [1,2].

The main chemical-physical and technological properties of asbestos minerals are resistance to abrasion, resistance to heat and to chemicals, flexibility, resiliency, and a low sound transmission coefficient [3]. Due to these outstanding characteristics, chrysotile $\text{Mg}_3\text{Si}_2\text{O}_5(\text{OH})_4$, amosite $(\text{Fe},\text{Mg})_7[(\text{OH})\text{Si}_4\text{O}_{11}]_2$ and crocidolite $\text{Na}_2\text{Fe}_3\text{Fe}_2[(\text{OH})\text{Si}_4\text{O}_{11}]_2$ were used from 1720 to the 1980s in numerous (more than 3000) industrial applications and for manufacturing various types of products known as asbestos-containing materials (ACMs). Although these minerals have good technological properties, if inhaled, they can cause several respiratory diseases [4]. For this reason, they are classified as carcinogenic substances Group 1 by the International Agency for Research on Cancer (IARC) [5], and many countries have banned their use [6]. Today, ACMs used in many countries must be safely disposed of or made inert. In the countries that have banned the use of asbestos minerals and where remediation policies are encouraged, many studies and patents have dealt with the possible disposal and re-use of ACMs [7–12]. The preference for recycling compared to landfill disposal is specified in the European Directive [13], since recycling is the best solution, as it reduces

environmental impact and the consumption of primary raw materials. In this regard, although the crystal-chemical transformation induced by the thermal treatment of asbestos is the most common transformation process [14–23], other processes such as biological treatment, dissolution by acid, thermochemical and mechano-chemical processes have been used for treating ACMs during the last two decades [24–32]. In particular, mechano-chemical treatment, which could be used for disposing of and/or recycling asbestos, is capable of increasing particle reactivity [33], reducing the sintering temperature [34] and reducing the thermal decomposition temperature [35,36]. In this regard, Suquet [37] has shown that grinding and/or leaching pre-treatment of chrysotile affected its dissolution in water. A mechano-chemical treatment was also successfully applied to asbestos by Plescia et al. [38], who showed how grinding can completely modify the fibrous morphology of asbestos.

The mechano-chemical treatment of chrysotile with a planetary ball mill was later applied by Inoue et al. [39], demonstrating how chrysotile was completely converted into non-fibrous amorphous material after 2–4 h of grinding. The so-called high-energy milling (HEM) has recently been demonstrated to be capable of ensuring amorphization of asbestos-containing waste (ACW) [40,41]. To date, studies concerning the mechano-chemical treatment of asbestos have been generally focused on chrysotile or chrysotile containing ACMs, being the only asbestos mineral still used worldwide. Such studies were not related to the thermal behaviour and no studies have been carried out on UICC standard amosite amphibole asbestos and UICC standard crocidolite amphibole asbestos, although it is well known that in countries like Italy ACMs may contain amosite and crocidolite in addition to chrysotile. Moreover, it is important to note that the destruction sequence related to the mechano-chemical treatment of ACW, consisting of various amorphous and crystalline phases [42], could differ from the destruction sequence of standard asbestos minerals. For example, the loss of CO₂ from the calcite present in cement leads to a reducing environment in the mill container, which can influence the transformation path of the phases involved in grinding [43]. Moreover, it is worth remembering that using different ball mill devices or the same ball mill under different conditions can provide totally different results [44,45].

In this context, this work focuses on the effects that dry grinding in an eccentric vibration mill has on representative samples of chrysotile from Balangero (Italy), UICC standard amosite and UICC standard crocidolite in terms of their crystallinity, temperature stability and fibre size when they are mechanically treated for 30 s, 5 min and 10 min. Adopting mechanical treatment to destroy the structure of asbestos has also been discussed in terms of using it in combination with thermal treatment which can be applied after milling. We believe this study could shed new light on the mechanisms of safe disposal of asbestos through the grinding process.

2. Materials and Methods

For the study, the following mineral fibres have been selected:

(1) chrysotile from Balangero (Italy) [(Mg_{5.81}Fe²⁺_{0.21}Al_{0.27}Fe³⁺_{0.03}Cr_{0.01})_{6.33}Si_{3.97}O₁₀(OH)_{7.11}], with minor impurities of diopside (CaMgSi₂O₆) and hematite (Fe₂O₃); (2) UICC (Union for International Cancer Control) standard amosite amphibole asbestos from Penge mine (South Africa) [(Ca_{0.02}Na_{0.01})(Fe²⁺_{5.36}Mg_{1.48}Fe³⁺_{0.11}Mn_{0.06})_{7.01}(Si_{7.93}Al_{0.01})_{7.94}O_{21.94}(OH)_{2.06}], with minor impurity of quartz (SiO₂); (3) UICC (Union for International Cancer Control) standard crocidolite amphibole asbestos from Koegas Mine, (South Africa) [(Na_{1.96}Ca_{0.03}K_{0.01})₂(Fe²⁺_{2.34}Fe³⁺_{2.05}Mg_{0.52})_{4.91}(Si_{7.84}Al_{0.02})_{7.86}O_{21.36}(OH)_{2.64}], with minor impurity of quartz (SiO₂). The crystallinity, thermal behaviour, and other features of these samples have been already published elsewhere [46–49]. Dry grinding of the samples (1 g) was conducted using a Bleuler Rotary Mill for 30 s, 5 and 10 min at a speed of 900 revolutions per min (rpm). The grinding container (with a capacity of 100 mL) has an anvil ring of 1285 g and puck of 1388 g to pulverize the sample by an eccentric vibratory motion in which the compression and the shear forces [50] are the main forces acting on the asbestos minerals. The measured container temperature does not exceed 60 °C during the grinding.

Samples were characterized using an X-ray powder diffractometer (Bruker D8 Advance model, Bruker, Billerica, MA, USA) operating at 40 kV and 40 mA and by recording scans in the range of $3\text{--}66^\circ 2\theta$, with a step size of $0.02^\circ 2\theta$ and time per step of 3 s. Thermogravimetry (TG) and differential scanning calorimetry (DSC) were performed in an alumina crucible under a constant aseptic air flow of 30 mL min^{-1} with a Netzsch STA 449 C Jupiter (Netzsch-Gerätebau GmbH, Selb, Germany) in the $25\text{--}1000^\circ\text{C}$ temperature range with a heating rate of $10^\circ\text{C min}^{-1}$ and 20 mg of sample powder. Instrumental precision was checked by 6 repeated collections on a kaolinite reference sample revealing good reproducibility (instrumental theoretical T precision of $\pm 1.2^\circ\text{C}$). Netzsch Proteus thermal analysis software (Netzsch-Gerätebau GmbH, Selb, Germany) was used to identify exo- and endothermic peaks, weight loss, onset, end temperatures and enthalpy of dehydroxylation (ΔH_{dehy}). It is worth remembering that the area under the exo- or endotherm on the measured DSC curve is proportional to the heat of reaction (ΔH) occurring at that temperature [51]. Transmission electron microscopy (TEM) was performed using a Jeol JEM 1400 Plus (Tokyo, Japan) working at 120 kV, equipped with a double tilt holder to check the morphology of the samples and to obtain structural data by selected area electron diffraction (SAED); an energy dispersive X-ray spectrometry (EDS) by Jeol allowed us to obtain analytical electron microanalyses (AEM). For TEM investigations, the sample was put in isopropyl alcohol; three drops of the obtained suspension were deposited on a copper mesh grid coated with 200 \AA carbon film.

3. Results

3.1. X-ray Diffraction Characterization

3.1.1. Chrysotile

The X-ray diffraction pattern of the 30 s mechanically ground chrysotile was characterized by sharp peaks (Figure 1), indicating a high level of crystallinity of the materials as already observed in previous studies [46]. After 5 min of grinding, all reflections disappeared except for the (002), (−111) and (004) reflections which were still visible due to texture effects, even if with remarkably reduced intensity (Figure 1).

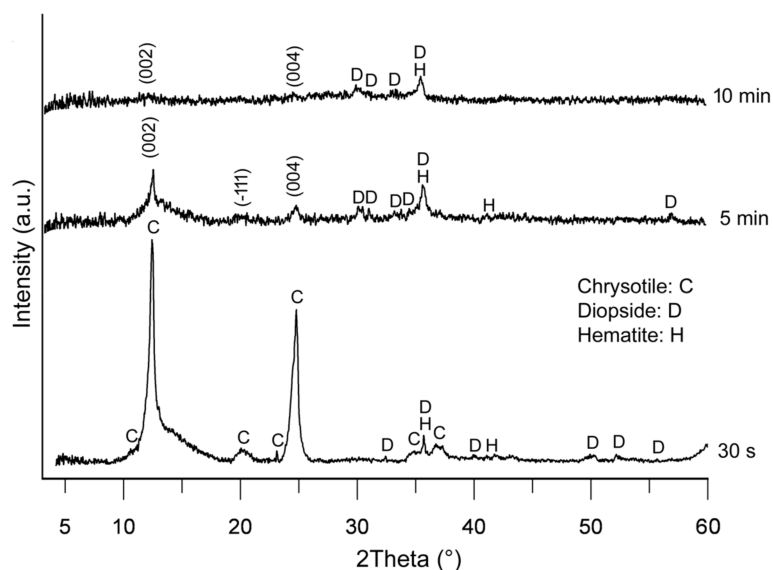


Figure 1. XRPD patterns of chrysotile recorded after 30 s, 5 min and 10 min of grinding time.

The increase in grinding time (i.e., 10 min) led to the disappearance of (−111) reflection and to a further significant decrease in intensity and broadening of the (002) and (004) peaks (Figure 1) indicating

that only poorly crystalline fibres were still present in the sample. Moreover, the diagnostic reflections of diopside $\text{CaMgSi}_2\text{O}_6$ (JCPDS card 41-1370) (present as an impurity in the sample), which were not detected after 30 s of grinding owing to the overlapping of chrysotile reflections, became visible after 5 and 10 min of grinding (Figure 1). Finally, hematite (Fe_2O_3), also originally identified by XRPD in the unground sample as an impurity, showed its typical (110) reflection (JCPDS card 24-0072) even after 10 min of grinding.

3.1.2. Amosite

After 30 s of grinding, amosite was highly crystalline with quartz present as an impurity (Figure 2). After 5 min of grinding, the XRPD pattern of the sample exhibited a characteristic amorphous trace except for (011) and (220) reflections with lower intensity than that of the sample ground for 30 s. After 10 min grinding, the (011) reflection disappeared from the pattern (Figure 2). It is evident that no crystalline amosite was detected by XRPD after 10 min of grinding. Mechanical grinding also affected the structure of quartz (JCPDS card 46-1045) whose intensity of characteristic (101) and (100) reflections decreased after grinding (Figure 2).

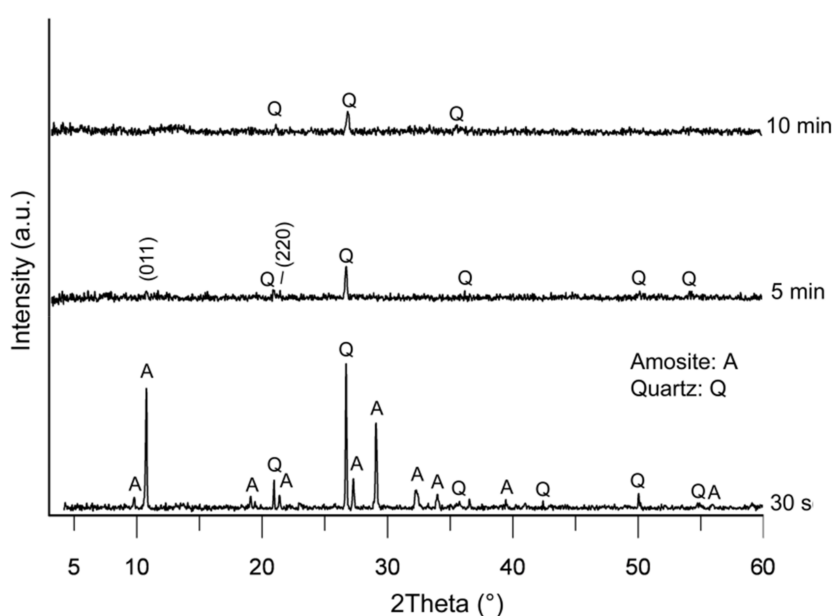


Figure 2. XRPD patterns of amosite recorded after 30 s, 5 min and 10 min of grinding time.

3.1.3. Crocidolite

Figure 3 shows sharp reflections of crocidolite after grinding for 30 s, in agreement with the results previously reported by Bloise et al. [46]. After 5 min of grinding, most of the crocidolite reflections disappeared, while (110), (040), (310), (151) and (-260) reflections are preserved although with much less intensity. When the grinding time was increased up to 10 min, broadening and a slight decrease in intensity were observed for all reflections except for the (040) reflection which was no longer present (Figure 3). This behaviour was diagnostic of crystal defect formation and of lower levels of crystallinity of the 10 min ground sample compared to the sample ground for 5 min (Figure 3). However, after 10 min of grinding, the X-ray diffraction patterns still showed a clearly visible (101) quartz reflection (JCPDS card 46-1045) present as an impurity in the sample (Figure 3).

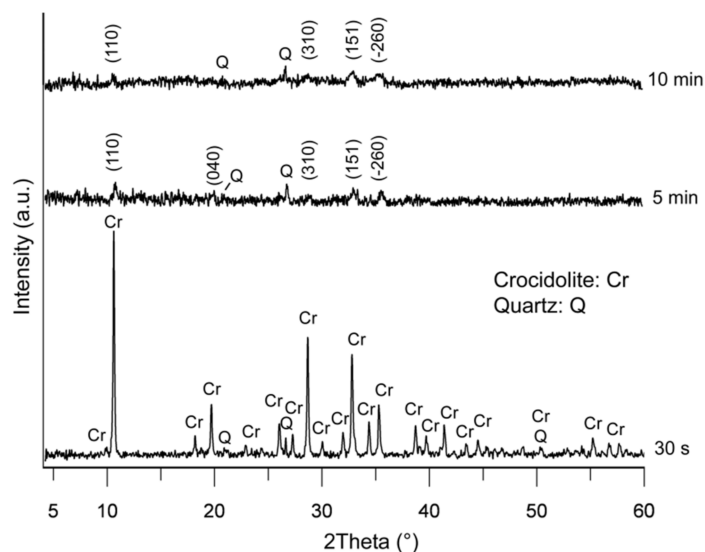


Figure 3. XRPD patterns of crocidolite recorded after 30 s, 5 min and 10 min of grinding time.

3.2. Thermal Analysis Characterization

3.2.1. Chrysotile

After 30 s of grinding, the DSC curve of the chrysotile (Figure 4) showed an endothermic event at 660 °C related to chrysotile dehydroxylation [46]. After 5 min of grinding, the structure of chrysotile collapsed at a lower temperature as shown by the endothermic peak at 625 °C, which shifted downward to 622 °C becoming weaker in the sample ground for 10 min (Figure 4).

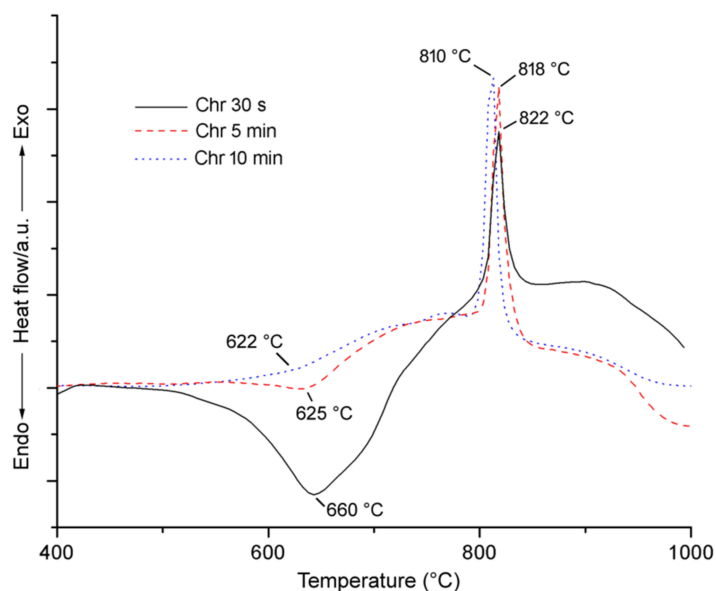


Figure 4. Differential scanning calorimetry of chrysotile after 30 s, 5 min and 10 min of grinding time.

The exothermic peaks on the DSC curves (822, 818 and 810 °C) indicate forsterite (Mg_2SiO_4) and enstatite (MgSiO_3) crystallization (e.g., [46,52]). Forsterite (JCPDS card 34-0189) and enstatite (JCPDS card 22-0714) were identified by XRPD as the main crystalline phases formed after combined grinding for 30 s, 5 and 10 min and thermal treatments at 1000 °C (Supplementary Figure S1).

The endothermic event at 660 °C displays an area under the peak (ΔH_{dehy}) of 345 J/g, which is related to the heat required for the dehydroxylation reaction of chrysotile (Table 1).

Table 1. Main peak temperatures in DSC curves and ΔH_{dehy} for chrysotile (Chr) ground for 30 s, 5 min and 10 min, w = weak, s = strong, endo = endothermic, exo = exothermic. The area under the endothermic peak (ΔH_{dehy}) is delimited in the range onset-end.

| Sample (Grinding Time) | Chr 30 s | Chr 5 min | Chr 10 min |
|------------------------|-------------------------|-----------------------|-------------------------|
| DSC T (°C) | 660 endo s 822 exo s | 625 endo 818 exo s | 622 endo w 810 exo s |
| ΔH (J/g) | 345 | 35 | 12 |
| Onset-end (°C) | 500–725 | 556–656 | 556–656 |

This value is in agreement with Weber and Greer [53], who reported an enthalpy of dehydroxylation (ΔH) of 341 and 346 J/g for chrysotile from Australia and Urals, respectively. The endothermic peak areas (ΔH) decreased significantly from 345 to 35 and 12 J/g as grinding time increased to 30 s, 5 and 10 min, respectively (Figure 5). In fact, the chrysotile DSC endothermic peak nearly disappeared after 10 min of grinding. After grinding for 30 s, the thermogravimetric (TG) curves of chrysotile recorded a weight loss of approximately 0.52% in the range between 40 and 110 °C due to the water adsorbed (Table 2). The weight loss, in the same temperature range (40–110 °C), increased to 2.67% as grinding time increased up to 5 min and then decreased to 1.08% after 10 min of grinding (Table 2).

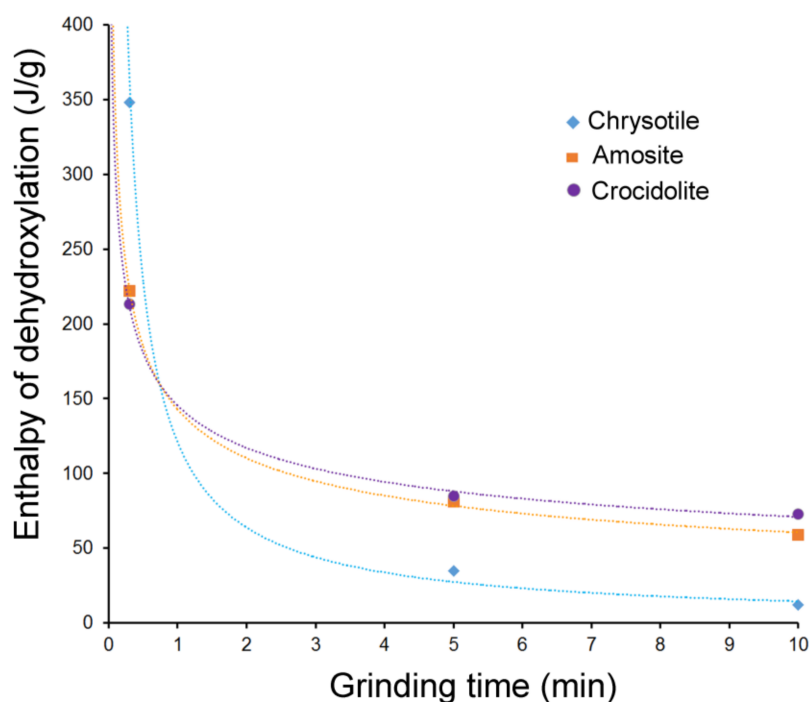


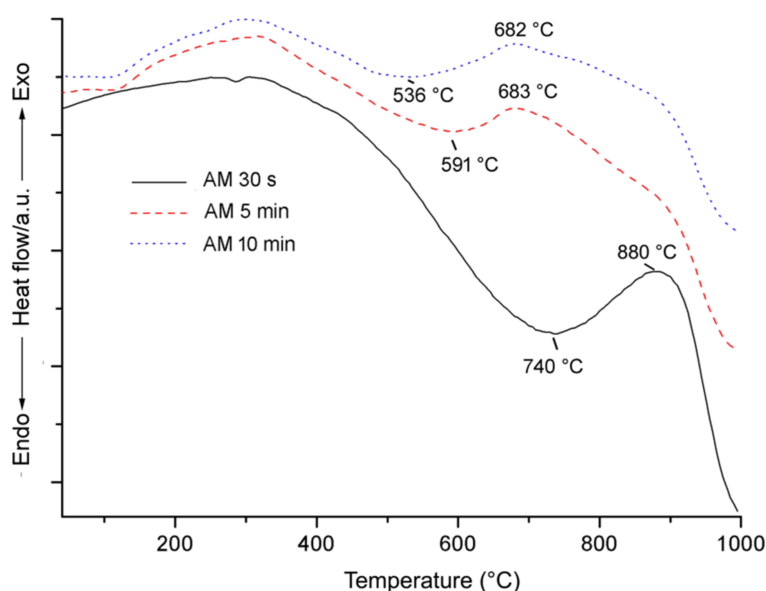
Figure 5. Change in enthalpy of dehydroxylation (ΔH_{dehy}) as grinding time increases.

Table 2. Thermogravimetric, mass loss (%) for chrysotile (Chr); amosite (AM); crocidolite (CR) in the range of 40–110 (°C) after grinding for 30 s, 5 min and 10 min.

| Grinding Time | 30 s | 5 min | 10 min |
|---------------|---------------------|---------------------|---------------------|
| | TG Loss (%) | | |
| | T Range 40–110 (°C) | T Range 40–110 (°C) | T Range 40–110 (°C) |
| Chr | 0.52 | 2.67 | 1.08 |
| AM | 0.14 | 0.50 | 0.42 |
| CR | 0.26 | 2.57 | 0.95 |

3.2.2. Amosite

In Figure 6 the broad endothermic effect at 740 °C was related to the structural breakdown of amosite after grinding for 30 s, in agreement with literature [53]. The temperature breakdown of amosite shifted downward to 591 °C if grinding was 5 min long (Table 3) with a further decrease to 536 °C when the sample was ground for 10 min.

**Figure 6.** Differential scanning calorimetry of amosite after 30 s, 5 min and 10 min of grinding.

After 30 s of grinding, the DSC curve shows a broad exothermic peak at 880 °C due to a pyroxene phase $(\text{Fe,Mg})_2\text{Si}_2\text{O}_6$ and hematite (Fe_2O_3) formation [54] which shifted to lower temperature as grinding time increased from 30 s to 5 min and 10 min (Figure 6; Table 3). After heating at 1000 °C, XRPD patterns of amosite ground for 5 min show the formation of hematite (JCPDS card 33-0664) and small amount of a pyroxene phase (JCPDS card 17-0548), while the main crystalline phases formed after heating the sample ground for 10 min were hematite, fayalite Fe_2SiO_4 (JCPDS card 9-0484) and ferrosilite FeSiO_3 (JCPDS card 26-0876) (Supplementary Figure S2). For amosite, the enthalpy of dehydroxylation (ΔH) decreased with elapsed grinding times from 222 to 81 and 59 J/g at 30 s, 5 min and 10 min, respectively (Table 3). In particular, after 5 min of grinding, the amount of energy required to cause the dehydroxylation of this phase decreased by 141 J/g compared to the energy required after 30 s of grinding process, while after 10 min the energy required only decreased by 22 J/g (Figure 5). The absorbed water (in the temperature range of 40–110 °C) on the amosite surface after 30 s of grinding, was 0.14% as detected by TG (Table 2). After 5 min of grinding, the absorbed water in the same temperature range increased to 0.50% while it decreased to 0.42% after 10 min of grinding (Table 2).

Table 3. Main peak temperatures for DSC curves and ΔH_{dehy} for amosite (AM) after grinding for 30 s, 5 min and 10 min, endo = endothermic, exo = exothermic. The area under the endothermic peak (ΔH_{dehy}) is delimited in the range onset-end.

| Sample (Grinding Time) | AM 30 s | AM 5 min | AM 10 min |
|------------------------|---------------------|---------------------|---------------------|
| DSC T (°C) | 740 endo 880 exo | 591 endo 683 exo | 536 endo 682 exo |
| ΔH (J/g) | 222 | 81 | 59 |
| Onset-end (°C) | 586–800 | 450–656 | 462–655 |

3.2.3. Crocidolite

As we can see from the DSC patterns (Figure 7), after 30 s of grinding, the thermal decomposition of crocidolite took place in the range 350–700 °C with two distinct endothermic events: the first stage at 374 °C is related to the partial dehydroxylation during which hydrogen ions and electrons were lost, to form an oxy-crocidolite (crocidolite partially dehydrogenated) [55], while the second endothermic effect at 650 °C represents the main dehydroxylation of crocidolite as already discussed in Bloise et al. [46]. The first endothermic peak was no longer observable when the sample was ground for 5 and 10 min. Nevertheless, as shown in Figure 7, the main peak related to crocidolite dehydroxylation shifted to lower temperatures as grinding time increased: from 650 °C to 555 °C and 538 °C in the samples ground for 30 s, 5 and 10 min, respectively.

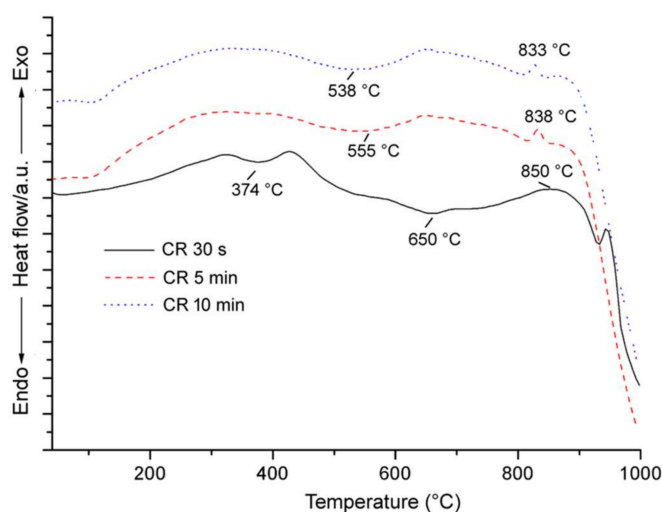


Figure 7. Differential scanning calorimetry of crocidolite after 30 s, 5 min and 10 min of grinding time.

Finally, after 30 s of grinding, crocidolite showed a broad exothermic DSC signal at approximately 850 °C which shifted to lower temperature and reduced its intensity in the samples ground for 5 and 10 min (Table 4). XRPD of ground samples heated to 1000 °C revealed the formation of hematite Fe_2O_3 (JCPDS card 33-0664), cristobalite SiO_2 (JCPDS card 1-0424) and aegirine $\text{NaFe}^{3+}\text{Si}_2\text{O}_6$ (JCPDS card 34-0185) while quartz SiO_2 , present as impurities in the starting sample, disappeared (supplementary Figure S3). The amount of aegirine is lower in the sample ground for 10 min, with characteristic reflections close to the detection limit. In regard to the enthalpy of dehydroxylation (ΔH_{dehy}), crocidolite behaves like amosite (Figure 5). ΔH decreased as grinding time increased as shown in Figure 5. The amount of heat required to cause the breakdown of crocidolite ground for 5 min (85 J/g) is approximately half of the value recorded for the sample ground for 30 s (213 J/g), but about a constant value was reached between 5 and 10 min of grinding time (Table 4). The absorbed water (in the temperature range of 40–110 °C) on the crocidolite surface after 30 s of grinding was

0.26% as detected by TG. After 5 min of grinding, the water absorbed in the same temperature range increased to 2.57% while it decreased to 0.95% after 10 min of grinding (Table 2).

Table 4. Main peak temperatures in DSC curves and ΔH_{dehy} for crocidolite (CR) after grinding for 30 s, 5 min and 10 min, w = weak, s = strong, endo = endothermic, exo = exothermic. The area under the endothermic peak (ΔH_{dehy}) is delimited in the range onset-end.

| Sample (Grinding Time) | CR 30 s | CR 5 min | CR 10 min |
|------------------------|------------------------|-------------------------|-------------------------|
| DSC T (°C) | 650 endo 850 exo w | 555 endo w 838 exo s | 538 endo w 833 exo s |
| ΔH (J/g) | 213 | 85 | 73 |
| Onset-end (°C) | 311–420 and 430–817 | 426–661 | 415–648 |

3.3. TEM Characterization

Figure 8 was obtained with low magnification TEM observation, in order to show the whole of grid opening in each micrograph.

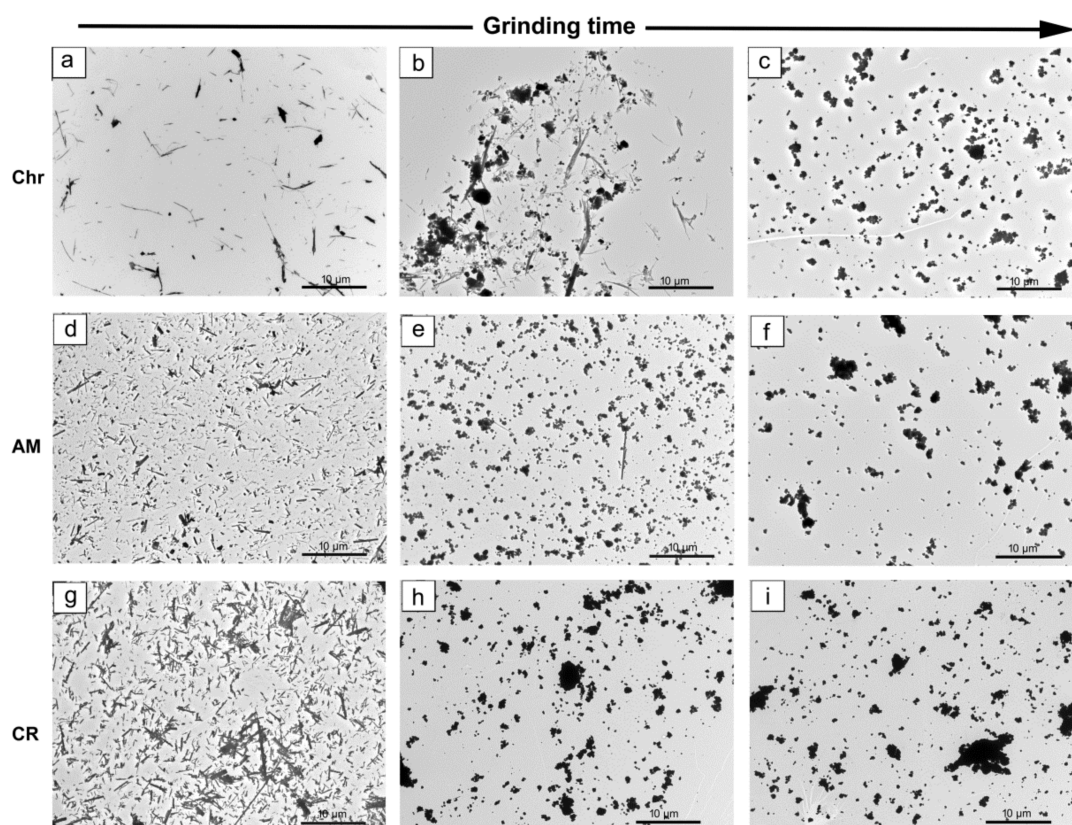


Figure 8. TEM images of: chrysotile (a–c); amosite (d–f); crocidolite (g–i). 30 s grinding (a,d,g); 5 min grinding (b,e,h); 10 min grinding (c,f,i).

3.3.1. Chrysotile

The chrysotile sample ground for 30 s showed the typical asbestiform crystal habit with single fibrils, and the hollow core running along the fibril axis. The chrysotile fibres were often curved and the length of some fibres may be longer than 10 μm . After 5 min of grinding, it is possible to observe many agglomerates of particles (Figure 8b) rich in Mg and Si, and minor Al and Fe

(AEM/TEM verified) and the appearance of diffuse halos in the corresponding SAED is indicative of a non-crystalline phase. In order to explain the reaction caused by grinding, it is important to remember that chrysotile is a trioctahedral hydrous layer silicate based on a 1:1 layer structure whose layers are rolled assuming a characteristic fibrous habit [56]. After 5 min of grinding, the original stacking layers were rolled out and delaminated; the lamellae were broken by mechanical impact thus causing a decrease in particle size and the formation of agglomerates of non-crystalline material.

However, flexible chrysotile bundles and many single fibres longer than 10 μm are preserved (Figure 9a).

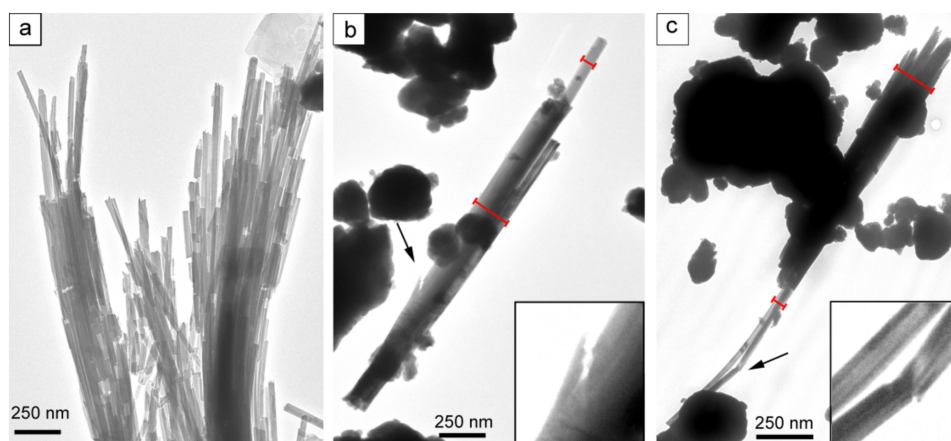


Figure 9. TEM images of: chrysotile (a); amosite (b); crocidolite (c) after 5 min of grinding. Arrows in (b,c) indicate the zoom area. The red lines in b and c indicate the diameter of the fibres.

The amount of non-crystalline particle agglomerates increases in the sample ground for 10 min (Figure 8c). However, at higher magnification, rare single chrysotile fibres with a maximum length of 1500 nm and width of 60 nm were still observed, all showing moderate crystallinity as proved by the diffraction dots and halos in the SAED patterns (Figure 10).

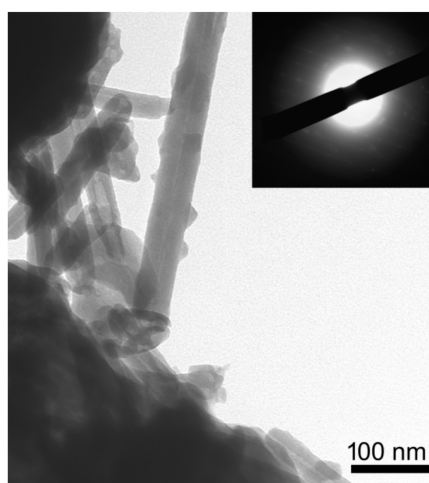


Figure 10. TEM image of chrysotile and corresponding SAED pattern after 10 min of grinding.

3.3.2. Amosite

TEM micrographs of ground amosite are presented in Figure 8d–f. Many fibres with typical prismatic rod-shaped morphology were found in the sample after 30 s of grinding, which had a maximum length of 15 μm . After 5 min of grinding, many particles chemically consistent with amosite

composition (AEM/TEM verified) but amorphous in nature (SAED patterns with full halo ring and rare diffraction spots) were detected. Few prismatic-shaped fibres with an average length of 8 μm can still be found (Figure 8e). Figure 9b shows how the grinding prompts the longitudinal splitting of the fibres parallel to (110) cleavage surfaces into thinner fibrils, reducing their width from approximately 200 to 60 nm (Figure 9b), and also causing the formation of fractures semi-perpendicular to the elongation of the fibres (Figure 9b). Many of them show the presence of chain-multiplicity faults defects (CMFs) developed along the elongation of the fibres [57]. Therefore, grinding causes longitudinal splitting from larger fibres into thinner fibrils preferentially along CMFs. As grinding progresses up to 10 min, only a few fibres with a maximum length of 1.2 μm were still visible (Figure 11), even if SAED confirmed that the crystallinity of these fibres remained even after long grinding treatments.

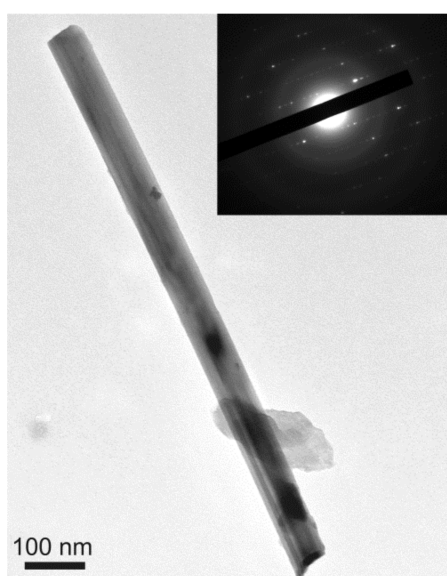


Figure 11. TEM image of amosite and corresponding SAED pattern after 10 min of grinding.

3.3.3. Crocidolite

Like amosite, crocidolite ground for 30 s shows a prismatic rod-shaped crystal habit and high crystallinity with some fibres that can also reach a length of 30 μm (Figure 8g). However, after grinding for 5 min, fibres longer than 3 μm are rare (Figure 8h). The majority of the fibres show breaking parallel to (110) cleavage surfaces and occasionally transverse to the fibre axis, leading to a decrease in diameter from approximately 370 to 40 nm (Figure 9c). A visual inspection by TEM of the 10 min grinding sample revealed the presence of some fibre aggregates with amorphous particles (Figure 8i) that were chemically composed of Si, Mg, Fe, Na as detected by AEM. The fibres were 1.7 μm long and preserved their habit and crystallinity as observed at high magnification (Figure 12).

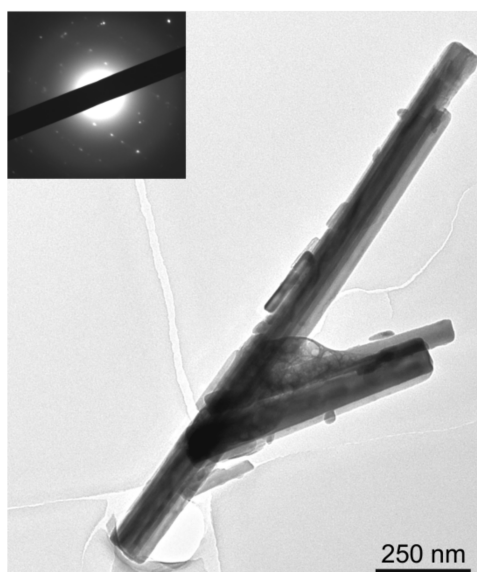


Figure 12. TEM image of crocidolite and corresponding SAED pattern after 10 min of grinding.

4. Discussion

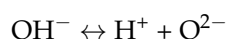
The XRPD patterns of the asbestos samples generally show similar features as the grinding process proceeds; a decrease in the intensity of all reflections and an increase in the background contribution are invariably observed, indicating amorphization of the crystal fibres. The abrupt intensity decrease of all reflections in the first 5 min of grinding indicates that the structure of asbestos is rapidly damaged by mechanical treatment. After 10 min of grinding, the XRPD patterns of chrysotile and crocidolite only showed minor broad reflections proving that most of fibres were made amorphous. Regarding amosite, the absence of peaks (Figure 2) in the corresponding X-ray diffraction pattern was not due to the complete destruction of the fibres after 10 min of grinding because small amounts of amosite have been detected by DSC and TEM. The existence of amosite preserved within the samples after 10 min grinding was not detected by XRPD because it was below the detection limit of the instrument.

The results of the thermal analysis show a relationship between the increase in grinding time from 30 s to 10 min and the endothermic DSC effects. Indeed, the reduction in particle size, the formation of lattice defects or stressed structures induced by grinding processes cause a downshift temperature of the original endothermic DSC effects. However, the decrease in temperature is stronger in amosite ground for 5 min than in crocidolite and chrysotile, thus proving that amosite is less resistant to grinding and thus markedly damaged. Furthermore, in crocidolite, grinding treatment for 5 and 10 min produces: (i) a disappearance of the first event at 374 °C related to the loss of hydrogen ions and electrons to give oxy-crocidolite [46] since the dehydrogenation process from a strongly altered structure had already been completed during grinding process as occurs for other silicates [58,59]; (ii) a decrease in second endothermic effect due to easier dehydroxylation from a strongly altered structure. Chrysotile and amosite decomposition took place essentially in one main endothermic effect. In chrysotile and amosite, grinding treatment for 5 and 10 min produced a decrease in endothermic effects due to easier dehydroxylation from strongly altered structures. The decomposition of amosite followed a very similar pattern to crocidolite although in this case the formation of oxy-amosite (anhydrous amosite) involved a dehydroxylation process as well as a dehydrogenation process that occur simultaneously [52], and thus, it was not possible to identify oxy-amosite by the dehydroxylation peak on the DSC curve. In fact, crocidolite may be unique amongst the asbestos amphiboles in that the dehydroxylation process, and the structural breakdown process were consecutive rather than concurrent [52].

When grinding chrysotile, amosite and crocidolite, some of the energy is used for particle breakage whilst part of the energy is stored in the minerals [60]. However, there were some limitations regarding energy storage. In fact, asbestos minerals have low thermal conductivity; therefore, the energy delivered is not stored as thermal energy but is applied to destroy the crystalline lattice. In fact, the samples were partially destroyed after 5 and 10 min of grinding. In order to completely destroy the original structure, an additional amount of thermal energy equal to enthalpy of dehydroxylation (ΔH_{dehy}) is required (corresponding to the area calculated under the DSC peak). It was observed that enthalpy of dehydroxylation (ΔH_{dehy}) decreased as grinding time increased (Figure 5). This implies that partially dehydroxylation already occurred during the grinding process as observed for kaolinite [59]; montmorillonite [58] and sepiolite [61]. This dehydroxylation is related with the loss of some OH groups through a prototropic mechanism based on the concept of protons migration during grinding and their consequent combination with hydroxyl groups to form water molecule. Prototropy produces a water molecule by the interaction of two hydroxyl groups in a two-step process as follows:



This reaction takes place when fibres are mechano-chemically activated. The effect of mechano-chemical activation is the point heating of the mineral, which causes the dehydroxylation of the mineral at contact points between the grinding medium and the mineral structure [62]. The point contact heating at specific sites results in the attainment of high temperatures sufficient to cause dehydroxylation as follows:



Chrysotile grinding for 30 s requires larger amounts of energy for dehydroxylation than amosite and crocidolite (Table 2) due to the following reasons: (i) chrysotile contains more structural water than the amphiboles; (ii) the morphological differences between chrysotile and amphiboles (i.e., amosite crocidolite), indeed in chrysotile the main diffusion path of water is along the fibril axis (b) while radial diffusion is unlikely [63]. After only 5 min grinding, it is observed a significant decrease in the energy required for the total dehydroxylation of the three minerals, especially as far as chrysotile is concerned (Figure 5), as a consequence of strong structural alteration in the 1:1 silicate layer. In fact, after 5 min of grinding, the original stacking layers rolled to assume the characteristic fibrous habit of chrysotile were delaminated; therefore, the diffusion of water molecules can occur in all directions and not only along the fibril axis. Amosite and crocidolite also develop new surfaces due to grinding from which the structural OH groups can be removed using less energy (Figure 5).

The formation of new active surfaces in the ground chrysotile, amosite and crocidolite leads also to an increase in reactivity resulting in the crystallization of new formed phases (e.g., forsterite) at lower temperatures. This behaviour has also been observed for other minerals undergoing to grinding such as kaolinite and apatite [64,65]. However, after grinding the samples up to 10 min, there is only a slight decrease in enthalpy of dehydroxylation (ΔH_{dehy}) (Figure 5) as after 5 min of grinding most fibres are destroyed. In the stages, up to 5 min of grinding for all asbestos samples, the mechanical treatment resulted in particle size reduction and consequently an increase of the specific surface area. This led to an enhanced water absorption below 110 °C on TG curves; indeed, the increase of surface area of the samples after grinding may cause rehydroxylation process, due to the adsorption of atmospheric water molecules [61,66]. However, for longer grinding times such as 10 min, the adsorbed water content below 110 °C decreased due to the agglomeration of the particles. In fact, as also observed by TEM, particle aggregation took place after 10 min of grinding leading to an increase of the mean diameter of the aggregated particles. This trend is similar to that observed in experiments carried out on the grinding of talc [67] and kaolinite [68].

As regards to fibre size detected by TEM, after grinding for up to 30 s, asbestos fibres are crushed into smaller particles with respect to the raw samples [46] while rare aggregates were

detected (Figure 8a,d,g). All crocidolite fibres measured in the samples ground for 5 min were smaller than 5 μm in length, and therefore not classified as regulated fibres according to the World Health Organization (WHO) and European law [1,2]. On the other hand, some fibres of chrysotile and amosite ground for 5 min still showed lengths $>5 \mu\text{m}$. After grinding for 10 min, all chrysotile and amosite fibres also became smaller than the regulated fibres. TEM results show that the final product obtained after 10 min of grinding is composed of non-crystalline particles and very few small fibres in all three samples. However, both the crystallinity and the chemical composition of these fibres are preserved. TEM micrographs of the samples show fewer fibres as milling progresses (Figure 8). These observations occurred simultaneously with: (i) the disappearance of diffraction peaks from the asbestos samples observed by XRPD; (ii) a reduction in the enthalpy of dehydroxylation of asbestos samples.

5. Conclusions

New data on thermal behaviour, crystallinity and size of chrysotile, amosite and crocidolite after grinding treatment are reported in this work. Crystallinity, thermal behaviour, size and other characteristics of chrysotile, amosite and crocidolite grinding for 30 s, 5 and 10 min were evaluated by X-ray powder diffraction, thermal analysis and TEM/AEM methods. This study showed that grinding of chrysotile, amosite and crocidolite causes: (i) shift to lower temperatures of asbestos breakdown due to the increase in lattice strain and the decrease in crystallinity; (ii) the decrease of the enthalpy of dehydroxylation (ΔH_{dehy}); (iii) a significant reduction in the amount and size of fibres in the samples.

Moreover, results show that, after 10 min of grinding, the chrysotile, amosite and crocidolite fibres were all below the dimensions that define a regulated fibre according to the WHO and European law [1,2]. This fact was never recognized in previous papers. For the first time, we demonstrated the possibility to decrease the enthalpy of dehydroxylation (ΔH_{dehy}) of chrysotile, amosite and crocidolite asbestos by increasing the time of grinding from 30 s to 10 min. This is a very important outcome, since the decrease in enthalpy means the possibility to destroy the fibres at lower temperatures than those used for the destruction of the mechanically untreated fibres. In other words, fibres with structural defects or partially destroyed require less thermal energy to be transformed into non-hazardous material. Five minutes of grinding before thermal treatment are sufficient to achieve a significant reduction of the amount of energy required to dehydroxylate chrysotile, amosite and crocidolite, since this quantity remains almost the same even after 10 min of grinding. The increase in specific surface area attributed to the reduction in particle size obtained after 5 min of grinding treatment could improve the results of chemical inertization of asbestos, as the higher reactivity of the particles produces a faster reaction to acids.

Supplementary Materials: The following are available online at <http://www.mdpi.com/2075-163X/8/4/135/s1>, Figure S1: XRPD diagrams after the heating at 1000 °C of chrysotile ground for 30 s, 5 min and 10 min. Newly formed phases: F = forsterite; E = enstatite; H = hematite already present as an impurity; Figure S2: XRPD diagrams after the heating at 1000 °C of amosite ground for 30 s, 5 min and 10 min. Newly formed phases: H = hematite, C = clinoferrosilite; F = fayalite; S = ferrosilite; Q = quartz already present as an impurity; Figure S3: XRPD diagrams after the heating at 1000 °C of crocidolite ground for 30 s, 5 min and 10 min. Newly formed phases: Cr = cristobalite; H = hematite; A = aegirine.

Acknowledgments: This research was conducted within the granted Italian National PROGETTO DI UNA UNITA' DI RICERCA (PRIN) 2010–2011—prot. 2010MKHT9B 004 "Interazione fra minerali e biosfera: conseguenze per l'ambiente e la salute umana".

Author Contributions: A.B. conceived the research and performed XRPD, DSC/TG and TEM/AEM measurements, analysed the results and wrote the manuscript; M.C. and A.F.G. analysed the results and wrote the manuscript.

Conflicts of Interest: The authors declare no conflict of interest.

References

1. World Health Organization (WHO). *Asbestos and Other Natural Mineral Fibres. Environmental Health Criteria*, 53; World Health Organization: Geneva, Switzerland, 1986; 194p.

2. The European Parliament and the Council of the European Union. Directive 2003/18/EC of the European Parliament and of the Council of 27 March 2003 amending Council Directive 83/477/EEC on the protection of workers from the risks related to exposure to asbestos at work. *Off. J. Eur. Union* **2003**, L97, 48–52.
3. Gualtieri, A.F. Mineral fibre-based building materials and their health hazards. In *Toxicity of Building Materials*; Pacheco-Torgal, F., Jalali, S., Fucic, A., Eds.; Woodhead Publishing: Cambridge, UK, 2012; pp. 166–195.
4. Røe, O.D.; Stella, G.M. Malignant pleural mesothelioma: History, controversy and future of a manmade epidemic. *Eur. Respir. Rev.* **2015**, *24*, 115–131. [[CrossRef](#)] [[PubMed](#)]
5. IARC. *Overall Evaluations of Carcinogenicity: An Updating of IARC Monographs Volumes 1 to 42*; IARC: Lyon, France, 1987; 440p.
6. Gualtieri, A.F. (Ed.) Introduction. In *Mineral Fibres: Crystal Chemistry, Chemical-Physical Properties, Biological Interaction and Toxicity*; European Mineralogical Union: London, UK, 2017; Volume 18, pp. 1–15.
7. Anastasiadou, K.; Axiotis, D.; Gidarakos, E. Hydrothermal conversion of chrysotile asbestos using near supercritical conditions. *J. Hazard. Mater.* **2010**, *179*, 926–932. [[CrossRef](#)] [[PubMed](#)]
8. Gualtieri, A.F.; Giacobbe, C.; Sardisco, L.; Saraceno, M.; Gualtieri, M.L.; Lusvardi, G.; Cavenati, C.; Zanatto, I. Recycling of the product of thermal inertization of cement–asbestos for various industrial applications. *Waste Manag.* **2011**, *31*, 91–100. [[CrossRef](#)] [[PubMed](#)]
9. Gualtieri, A.F.; Boccaletti, M. Recycling of the product of thermal inertization of cement–asbestos for the production of concrete. *Constr. Build. Mater.* **2011**, *25*, 3561–3569. [[CrossRef](#)]
10. Viani, A.; Gualtieri, A.F. Recycling the product of thermal transformation of cement-asbestos for the preparation of calcium sulfoaluminate clinker. *J. Hazard. Mater.* **2013**, *260*, 813–818. [[CrossRef](#)]
11. Viani, A.; Gualtieri, A.F. Preparation of magnesium phosphate cement by recycling the product of thermal transformation of asbestos containing wastes. *Cem. Concr. Res.* **2014**, *58*, 56–66. [[CrossRef](#)]
12. Kusiorowski, R.; Zaremba, T.; Piotrowski, J.; Podwórny, J. Utilisation of cement-asbestos wastes by thermal treatment and the potential possibility use of obtained product for the clinker bricks manufacture. *J. Mater. Sci.* **2015**, *50*, 6757–6767. [[CrossRef](#)]
13. The European Parliament and the Council of the European Union. Directive 2008/98/EC of the European Parliament and of the Council of 19 November 2008 on waste and repealing certain Directives (Text with EEA relevance). *Off. J. Eur. Union* **2008**, L312, 3–30.
14. Gualtieri, A.F.; Tartaglia, A. Thermal decomposition of asbestos and recycling in traditional ceramics. *J. Eur. Ceram. Soc.* **2000**, *20*, 1409–1418. [[CrossRef](#)]
15. Leonelli, C.; Veronesi, P.; Boccaccini, D.N.; Rivasi, M.R.; Barbieri, L.; Andreola, F.; Lancellotti, I.; Rabitti, D.; Pellacani, G.C. Microwave thermal inertisation of asbestos containing waste and its recycling in traditional ceramics. *J. Hazard. Mater.* **2006**, *135*, 149–155. [[CrossRef](#)] [[PubMed](#)]
16. Gualtieri, A.F.; Cavenati, C.; Zanatto, I.; Meloni, M.; Elmi, G.; Gualtieri, M.L. The transformation sequence of cement–asbestos slates up to 1200 °C and safe recycling of the reaction product in stoneware tile mixtures. *J. Hazard. Mater.* **2008**, *152*, 563–570. [[CrossRef](#)] [[PubMed](#)]
17. Dellisanti, F.; Rossi, P.L.; Valdrè, G. Remediation of asbestos containing materials by Joule heating vitrification performed in a pre-pilot apparatus. *Int. J. Miner. Process.* **2009**, *91*, 61–67. [[CrossRef](#)]
18. Giacobbe, C.; Gualtieri, A.F.; Quartieri, S.; Rinaudo, C.; Allegrina, M.; Andreozzi, G.B. Spectroscopic study of the product of thermal transformation of chrysotile-asbestos containing materials (ACM). *Eur. J. Mineral.* **2010**, *22*, 535–546. [[CrossRef](#)]
19. Viani, A.; Gualtieri, A.F.; Pollastri, S.; Rinaudo, C.; Croce, A.; Urso, G. Crystal chemistry of the high temperature product of transformation of cement-asbestos. *J. Hazard. Mater.* **2013**, *248*, 69–80. [[CrossRef](#)] [[PubMed](#)]
20. Croce, A.; Allegrina, M.; Trivero, P.; Rinaudo, C.; Viani, A.; Pollastri, S.; Gualtieri, A.F. The concept of ‘end of waste’ and recycling of hazardous materials: In depth characterization of the product of thermal transformation of cement-asbestos. *Mineral. Mag.* **2014**, *78*, 1177–1191. [[CrossRef](#)]
21. Yamamoto, T.; Kida, A.; Noma, Y.; Terazono, A.; Sakai, S. Evaluation of thermally treated asbestos based on fiber number concentration determined by transmission electron microscopy. *J. Mater. Cycles Waste Manag.* **2016**, *20*, 214–222. [[CrossRef](#)]
22. Pawełczyk, A.; Bożek, F.; Grabas, K.; Chęćmanowski, J. Chemical elimination of the harmful properties of asbestos from military facilities. *Waste Manag.* **2017**, *61*, 377–385. [[CrossRef](#)] [[PubMed](#)]

23. Witek, J.; Kusiorowski, R. Neutralization of cement-asbestos waste by melting in an arc-resistance furnace. *Waste Manag.* **2017**, *69*, 336–345. [[CrossRef](#)] [[PubMed](#)]
24. Sugama, T.; Sabatini, R.; Petrakis, L. Decomposition of chrysotile asbestos by fluorosulfonic acid. *Ind. Eng. Chem. Res.* **1998**, *37*, 79–88. [[CrossRef](#)]
25. Candela, P.A.; Crummett, C.D.; Earnest, D.J.; Frank, M.R.; Wylie, A.G. Low-pressure decomposition of chrysotile as a function of time and temperature. *Am. Mineral.* **2007**, *92*, 1704–1713. [[CrossRef](#)]
26. Yanagisawa, K.; Kozawa, T.; Onda, A.; Kanazawa, M.; Shinohara, J.; Takami, T.; Shiraishi, M. A novel decomposition technique of friable asbestos by CHCl₃-decomposed acidic gas. *J. Hazard. Mater.* **2009**, *163*, 593–599. [[CrossRef](#)] [[PubMed](#)]
27. Yvon, Y.; Sharrock, P. Characterization of thermochemical inactivation of asbestos containing wastes and recycling the mineral residues in cement products. *Waste Biomass Valoriz.* **2011**, *2*, 169–181. [[CrossRef](#)]
28. Belardi, G.; Piga, L. Influence of calcium carbonate on the decomposition of asbestos contained in end-of-life products. *Thermochim. Acta* **2013**, *573*, 220–228. [[CrossRef](#)]
29. Yao, M.; Lian, B.; Teng, H.H.; Tian, Y.; Yang, X. Serpentine dissolution in the presence of bacteria *Bacillus mucilaginosus*. *Geomicrobiol. J.* **2013**, *30*, 72–80. [[CrossRef](#)]
30. Spasiano, D.; Pirozzi, F. Treatments of asbestos containing wastes. *J. Environ. Manag.* **2017**, *204*, 82–91. [[CrossRef](#)] [[PubMed](#)]
31. Spasiano, D.; Luongo, V.; Petrella, A.; Alfè, M.; Pirozzi, F.; Fratino, U.; Piccinni, A.F. Preliminary study on the adoption of dark fermentation as pretreatment for a sustainable hydrothermal denaturation of cement-asbestos composites. *J. Clean. Prod.* **2017**, *166*, 172–180. [[CrossRef](#)]
32. Spasiano, D. Dark fermentation process as pretreatment for a sustainable denaturation of asbestos containing wastes. *J. Hazard. Mater.* **2018**, *349*, 45–50. [[CrossRef](#)] [[PubMed](#)]
33. Berbenni, V.; Marini, A.; Bruni, G. Effect of mechanical milling on solid state formation of BaTiO₃ from BaCO₃-TiO₂ (rutile) mixtures. *Thermochim. Acta* **2001**, *374*, 151–158. [[CrossRef](#)]
34. Miriello, D.; Bloise, A.; Crisci, G.M.; Barrese, E.; Apollaro, C. Effects of milling: A possible factor influencing the durability of historical mortars. *Archaeometry* **2010**, *52*, 668–679. [[CrossRef](#)]
35. Sánchez-Soto, P.J.; Carmen Jiménez de Haro, M.; Pérez-Maqueda, L.A.; Varona, I.; Pérez-Rodríguez, J.L. Effects of dry grinding on the structural changes of kaolinite powders. *J. Am. Ceram. Soc.* **2000**, *83*, 1649–1657. [[CrossRef](#)]
36. Haurie, L.; Fernandez, A.I.; Velasco, J.I.; Chimenos, J.M.; Lopez-Cuesta, J.M.; Espiell, F. Effects of milling on the thermal stability of synthetic hydromagnesite. *Mater. Res. Bull.* **2007**, *42*, 1010–1018. [[CrossRef](#)]
37. Suquet, H. Effects of dry grinding and leaching on the crystal structure of chrysotile. *Clays Clay Miner.* **1989**, *37*, 439–445. [[CrossRef](#)]
38. Plescia, P.; Gizzi, D.; Benedetti, S.; Camilucci, L.; Fanizza, C.; De Simone, P.; Paglietti, F. Mechanochemical treatment to recycling asbestos-containing waste. *Waste Manag.* **2003**, *23*, 209–218. [[CrossRef](#)]
39. Inoue, R.; Kano, J.; Shimme, K.; Saito, F. Safe decomposition of asbestos by mechano-chemical reaction. *Mater. Sci. Forum* **2007**, *561*, 2257–2260. [[CrossRef](#)]
40. Hashimoto, S.; Takeda, H.; Okuda, A.; Kambayashi, A.; Honda, S.; Iwamoto, Y.; Fukuda, K. Detoxification of industrial asbestos waste by low-temperature heating in a vacuum. *J. Ceram. Soc. Jpn.* **2008**, *116*, 242–246. [[CrossRef](#)]
41. Colangelo, F.; Cioffi, R.; Lavorgna, M.; Verdolotti, L.; De Stefano, L. Treatment and recycling of asbestos-cement containing waste. *J. Hazard. Mater.* **2011**, *195*, 391–397. [[CrossRef](#)] [[PubMed](#)]
42. Viani, A.; Gualtieri, A.F.; Secco, M.; Peruzzo, L.; Artioli, G.; Cruciani, G. Minerals in the Human. Body Crystal chemistry of cement-asbestos. *Am. Mineral.* **2013**, *98*, 1095–1105. [[CrossRef](#)]
43. Martinelli, G.; Plescia, P. Mechanochemical dissociation of calcium carbonate: Laboratory data and relation to natural emissions of CO₂. *Phys. Earth Planet. Inter.* **2004**, *142*, 205–214. [[CrossRef](#)]
44. Weeber, A.W.; Haag, W.J.; Wester, A.; Bakker, H. Differences in the amorphization reaction by mechanical alloying of Ni-Zr resulting from different ball-milling techniques. *J. Less Common Met.* **1988**, *140*, 119–127. [[CrossRef](#)]
45. Eckert, J.; Schultz, L.; Hellstern, E.; Urban, K. Glass-forming range in mechanically alloyed Ni-Zr and the influence of the milling intensity. *J. Appl. Phys.* **1988**, *64*, 3224–3228. [[CrossRef](#)]
46. Bloise, A.; Catalano, M.; Barrese, E.; Gualtieri, A.F.; Gandolfi, N.B.; Capella, S.; Belluso, E. TG/DSC study of the thermal behaviour of hazardous mineral fibres. *J. Therm. Anal. Calorim.* **2016**, *123*, 2225–2239. [[CrossRef](#)]

47. Bloise, A.; Barca, D.; Gualtieri, A.F.; Pollastri, S.; Belluso, E. Trace elements in hazardous mineral fibres. *Environ. Pollut.* **2016**, *216*, 314–323. [[CrossRef](#)] [[PubMed](#)]
48. Pollastri, S.; Perchiazzi, N.; Lezzerini, M.; Plaisier, J.; Cavallo, A.; Dalconi, M.; Bursi Gandolfi, N.; Gualtieri, A. The crystal structure of mineral fibres. 1. Chrysotile. *Period. Mineral.* **2016**, *85*, 249–259.
49. Pollastri, S.; Perchiazzi, N.; Gigli, L.; Cavallo, A.; Bursi Gandolfi, N.; Pollok, K.; Gualtieri, A. The crystal structure of mineral fibres. 2. Amosite and fibrous anthophyllite. *Period. Mineral.* **2017**, *86*, 55–65.
50. González, G.; Sagarzazu, A.; Villalba, R. Study of the mechano-chemical transformation of goethite to hematite by TEM and XRD. *Mater. Res. Bull.* **2000**, *35*, 2295–2308. [[CrossRef](#)]
51. Liang, S.H.; Cameron, L.E. *Differential Scanning Calorimetry (DSC) for the Analysis of Activated Carbon*; Report No. 1098; Defense Research Establishment: Ottawa, ON, Canada, 1991.
52. Bloise, A.; Kusiorowski, R.; Lassinantti Gualtieri, M.; Gualtieri, A.F. Thermal behaviour of mineral fibres. In *Mineral Fibres: Crystal Chemistry, Chemical-Physical Properties, Biological Interaction and Toxicity*; Gualtieri, A.F., Ed.; European Mineralogical Union: London, UK, 2017; Volume 18, pp. 215–252.
53. Weber, J.N.; Greer, R.T. Dehydration of serpentine-heat of reaction and reaction kinetics at p H₂O = 1 atm. *Am. Mineral.* **1965**, *50*, 450–464.
54. Kusiorowski, R.; Zaremba, T.; Piotrowski, J.; Adamek, J. Thermal decomposition of different types of asbestos. *J. Therm. Anal. Calorim.* **2012**, *109*, 693–704. [[CrossRef](#)]
55. Hodgson, A.A.; Freeman, A.G.; Taylor, H.F.W. The thermal decomposition of crocidolite from Koegas. South Africa. *Mineral. Mag.* **1965**, *35*, 5–30. [[CrossRef](#)]
56. Whittaker, E.J.W. The structure of chrysotile. V. Diffuse reflections and fibre texture. *Acta Crystallogr.* **1957**, *10*, 149–156. [[CrossRef](#)]
57. Bloise, A.; Fornero, E.; Belluso, E.; Barrese, E.; Rinaudo, C. Synthesis and characterization of tremolite asbestos fibres. *Eur. J. Mineral.* **2008**, *20*, 1027–1033. [[CrossRef](#)]
58. Čičel, B.; Kranz, G. Mechanism of montmorillonite structure degradation by percussive grinding. *Clay Miner.* **1981**, *16*, 151–162. [[CrossRef](#)]
59. Horváth, E.; Frost, R.L.; Makó, É.; Kristóf, J.; Cseh, T. Thermal treatment of mechanochemically activated kaolinite. *Thermochim. Acta* **2003**, *404*, 227–234. [[CrossRef](#)]
60. Iguchi, Y.; Senna, M. Mechanochemical polymorphic transformation and its stationary state between aragonite and calcite I. Effects of preliminary annealing. *Powder Technol.* **1985**, *43*, 155–162. [[CrossRef](#)]
61. Cornejo, J.; Hermosin, M.C. Structural alteration of sepiolite by dry grinding. *Clay Miner.* **1988**, *23*, 391–398. [[CrossRef](#)]
62. Miller, J.G.; Oulton, T.D. Prototropy in kaolinite during percussive grinding. *Clays Clay Miner.* **1970**, *18*, 313–323. [[CrossRef](#)]
63. Cattaneo, A.; Gualtieri, A.F.; Artioli, G. Kinetic study of the dehydroxylation of chrysotile asbestos with temperature by in situ XRPD. *Phys. Chem. Miner.* **2003**, *30*, 177–183. [[CrossRef](#)]
64. Aglietti, E.F.; Lopez, J.P.; Pereira, E. Mechanochemical effects in kaolinite grinding. I. Textural and physicochemical aspects. *Int. J. Miner. Process.* **1986**, *16*, 125–133. [[CrossRef](#)]
65. Al-Wakeel, M.I. Effect of mechanical treatment on the mineralogical constituents of Abu-Tartour phosphate ore, Egypt. *Int. J. Miner. Process.* **2005**, *75*, 101–112. [[CrossRef](#)]
66. Henmi, T.; Yoshinaga, N. Alteration of imogolite by dry grinding. *Clay Miner.* **1981**, *16*, 139–149. [[CrossRef](#)]
67. Dellisanti, F.; Valdrè, G.; Mondonico, M. Changes of the main physical and technological properties of talc due to mechanical strain. *Appl. Clay Sci.* **2009**, *42*, 398–404. [[CrossRef](#)]
68. Juhasz, A.Z.; Opczky, L. *Mechanical Activation of Minerals by Grinding: Pulverizing and Morphology of Particles*; Akadémiai Kiadó: Budapest, Hungary, 1990; 234p.

